Processing and characterization of UHWMPE composite fibers with alumina particles in poly(ethylene-vinyl acetate) matrix

Jelena Zec[1], Nataša Tomić[2*], Milorad Zrilić[1], Smilja Marković[3], Dušica Stojanović[1] and Radmila Jančić-Heinemann[1]

[1]University of Belgrade, Faculty of Technology and Metallurgy, Belgrade, Serbia
[2]University of Belgrade, Innovation Center of Faculty of Technology and Metallurgy, Belgrade, Serbia
[3]Institute of Technical Sciences of SASA, Belgrade, Serbia

[*]**Corresponding author:** Nataša Tomić, University of Belgrade, Innovation Center of Faculty of Technology and Metallurgy, Belgrade, Serbia.
Email: ntomic@tmf.bg.ac.rs

Abstract

Processing of hybrid composites represents a challenge for engineers where the aim is to establish compatibility among several materials. The aim of this study is to evaluate the effects of different size and morphology of alumina fillers on the mechanical and thermal properties of the composite fibers based on ultra-high molecular weight polyethylene fibers (UHMWPE).These fibers have an outstanding elastic modulus and they are compatible with nonpolar sequences of the poly(ethylene-co-vinyl acetate) (EVA) matrix. Compared to the fibers, inferior mechanical properties of the matrix can be improved using alumina particles. Commercial Al_2O_3 nanoparticles, commercial whiskers and synthesized particles of Al_2O_3 doped with iron oxide, incorporated in different weight percent were used as fillers. The UHMWPE fibers were impregnated using the solution of EVA in toluene with dispersed particles. FT-IR and FE-SEM were

used for structural examination. Tensile testing revealed increasing of modulus of elasticity and strengths of obtained hybrid composite fibers. Thermal gravimetry showed improved thermal stability up to 350°C of the hybrid composite fibers with alumina particles doped with iron oxide. Results of tested samples showed that the best mechanical properties were for hybrid composite fibers with 1 wt.% of iron doped alumina filler.

Keywords

UHMWPE,Al_2O_3 reinforcement, EVA matrix, hybrid composite fibers, thermal stability

Introduction

Fiber-reinforced polymer composites are widely used due to their excellent properties, such as light weights, high tensile strength and moduli.[1]Poly(ethylene-co-vinyl acetate) (EVA) is a random copolymer synthesized by copolymerization of ethylene and vinyl acetate monomers with different acetate contents.[2] Due to their properties and processing characteristics, these copolymers have extensive applications in biomedical, food industry, construction, transport, wire and cable industry. They are commonly used as adhesives, electrical insulation, corrosion protection, waterproofing and packaging.[2-4]As adhesives, EVA copolymers are often used in combination with different types of materials like wood, rubber, metals, glass and polymers.[5,6]EVA properties depend on the content of each comonomer. Crystallization and melting characteristics of EVA are very sensitive to the VA content.[7]The melting temperature and degree of crystallinity decreases with an increase of vinyl acetate groups, but the glass transition temperature (T_g) increases with the increase of vinyl acetate content.[5-8]Presence of ethylene segments in EVA molecules provides characteristic to „plasticized" and increases the activity.[9]

The mechanical properties of the EVA as matrix are inferior compared to the fibers like ultra-high molecular weight polyethylene (UHWMPE) and they can be improved using inorganic fillers having a different morphology. The main reason to incorporate inorganic particles into polymer matrices is to obtain a composite with improved

mechanical properties like tensile strength, hardness, Young's modulus or stiffness applying different reinforcement mechanisms.[10]

A material that is widely used in composites is UHMWPE with long chains that provide sufficient load transfer between the macromolecules.[11]Due to its wear resistant characteristics, chemical inertness, strength, high impact resistance, toughness, tensile strength and excellent modulus, it has become one of the most modified polymers.[12]The most significant characteristics include high specific fiber strength that is about fifteen times stronger than steel. These advancements have led to the development of high performance polymer matrix composites.[13]The combination of high tensile strength, stiffness, low density and damage tolerance made UHMWPE fibers an ideal material. Ropes and cables made of this material have various applications for kites, fishing lines, offshore mooring etc.[11] The extreme tensile strength and the possibility to apply thick cables allow overdesign of the cable up to load carrying capacity of a few tons.

UHMWPE fibers have lack polarity and, therefore, it is not easy to produce composites due to the poor interfacial bonding with the matrix. On the other side, lateral interactions between molecules are the result of Van der Waals forces. Their presence in composite materials helps transferring off-axis loads retaining good mechanical properties along the fiber axis.[14]Although UHMWPE fibers have numerous useful characteristics and provide a load-bearing effect, their weakness is poor thermal resistance. In hybrid composite fibers the function of polymer is to transfer load to the

reinforcement and protect it from chemical and high temperature influences.[15]For this purpose, the most commonly used thermosetting resins are epoxy, but brittle, low impact resistance and low toughness, limits their usage. Weaknesses of epoxy resins can be overcome with the incorporation of the reinforcement phase such as UHMWPE fibers. [16]

In order to investigate the behavior of materials with different fillers, considerable studies have been conducted. That includes zirconium particles, TiO_2, kaolin, Al_2O_3, carbon fibers, carbon nanotubes (CNT), etc.. [12]Combination of organic and inorganic components and obtaining new materials attract increasing attention, since they combine the properties of including constituents.[17]

Bo Jin *et. al* have studied the composites where EVA is used as the polymer matrix and alumina nanoparticles as fillers. There was no agglomeration for 1.5wt.% of Al_2O_3 nanoparticles. The influence of the Al_2O_3 content on the tensile strength of EVA/Al_2O_3 nanocomposites showed increasing values up to 1.5wt.% of Al_2O_3 and at a higher content, the tensile strength starts to decrease, probably due to the agglomeration of nanoparticles.[18]Baskaran et al.[19] studied the effect of alumina nanoparticles in the mechanical properties of the nanocomposites. Chee et al.[20] noticed that the higher amount of alumina nanoparticles would reduce the reinforcing effect and mechanical properties of the composite due to poor dispersion and agglomeration.

In this work, different alumina fillers have been chosen due to their specific properties including hardness, wear resistance, high elastic modulus, thermal stability, high adsorption capacity, good thermal conductivity, high strength and stiffness, and good resistance to chemical and thermal environments.

Aluminum oxide has several crystal forms, and corundum is one of the most desired form for the reinforcement of composite materials when mechanical properties are important. Considering that α-$Al_2O_3$is the hardest form of alumina, it was a good choice to be used as reinforcement in order to improve the mechanical and thermal properties of polymer matrix composites. Like the other metal oxides, when Al_2O_3 is exposed to the atmosphere, its surface becomes covered with water in the form of the terminal OH groups.[21] Fine alumina particles exert influence on mechanical properties of the composite, even if the quantity is rather small.[22]Opeltet al. reported that after the addition of 0.15wt.%,0.50wt.% and 1.50wt.% of alumina, the modulus of elasticity had increased respectively. For tensile strength the results showed that there is no significant variation between the neat matrix and nanocomposite with small amount of Al_2O_3 fillers.[23]According to Wetzel et al. the similar behavior is observed for nanocomposites with up to 1% volume fraction (approximately 3.5 wt.%) of alumina fillers. On the other hand flexural modulus and strength depends on the filler volume fraction.[24]

Particle sizes at micro scale have a low influence on the Young's modulus. However, at nanoscale, Young's modulus of the composite increases as the size of particles

decreases. It was also reported that tensile strength decreases in composites with 3 vol.% nanoparticles, due to poor dispersion. Conversely, at 1 vol.% loading of microparticles, the tensile strength increases.[25]In the case of the Al_2O_3/epoxy nanocomposites, the formation of an interconnected network formed by the alumina nanoparticles was given as the main reason for the elastic modulus enhancements.[26]However, the elastic modulus in nanocomposites does not increase continuously with increasing the weight percentage of fillers. After the optimum weight percentage is reached, due to stress concentration, the elastic modulus will decrease.[27]

The aim of the present work is to research the properties of UHWMPE hybrid composite in poly (ethylene-co-vinyl acetate) matrix modified by commercial nanoparticles and whiskers of Al_2O_3 as fillers, and comparing the properties of composite in case of using new synthesized particles of alumina doped with iron oxide. Based on the results, the application of the hybrid composite material with the best characteristics will also be examined.

Experimental

Materials

The polyethylene used in this study was UHWMPE – DSM Dyneema, Netherlands (SK75, filament diameter 20 μm, density 0.970 g/cm^3). Commercial EVA (Elvax® 410) produced by DuPont™, containing 18 wt.% of vinyl acetate was chosen as a polymer

matrix. Commercial toluene (produced by Zorka Šabac) was used as a solvent. The aluminum oxide nanoparticles (< 50 nm particle size) and alumina whiskers (diameter 2-4 nm × 400 nm) were commercially supplied from Sigma Aldrich. Aluminum chloride hydroxide (Locron L) was purchased from the Clariant Company in the crystallized state of $Al_2Cl(OH)_5 \cdot 2.5 \cdot H_2O$. This product contained 23.5% Al_2O_3, 8.18% Cl, corresponding to an Al/Cl, molar ratio of 2/1. Iron chloride ($FeCl_3$) was also purchased from the same company.

Methods

Alumina particles doped with iron oxide were synthesized via sol-gel technique by the hydrolysis of aluminium ion. Solution of aluminum chloride hydroxide and iron chloride in water was mixed in a weight ratio of 19.5 g $Al_2(OH)_5Cl$, 0.5 g $FeCl_3$ and 15 g H_2O. Obtained gel was calcined for 2 hours on 900°C.[28]The mixture was grinded in a mortar and then sifted through a sieve. Nanoparticles, whiskers and synthesized particles of Al_2O_3 doped with iron oxide were annotated as n-Al_2O_3, w-Al_2O_3 and Fe-Al_2O_3. Obtained hybrid composite fibers with iron doped particles, alumina nanoparticles and alumina whiskers in UHMWPE fibers hybrid composite in EVA matrix were annotated as 1Fe-Al_2O_3/EVA/UHMWPE, 3Fe-Al_2O_3/EVA/UHMWPE, 5Fe-Al_2O_3/EVA/UHMWPE, 1n-Al_2O_3/EVA/UHMWPE, 3n-Al_2O_3/EVA/UHMWPE, 5n-Al_2O_3/EVA/UHMWPE, 1w-Al_2O_3/EVA/UHMWPE, 3w-Al_2O_3/EVA/UHMWPE,

5w-Al_2O_3/EVA/UHMWPE for the addition of 1 wt.%, 3 wt.% and 5 wt.% of the particles, respectively.

To obtain solutions with 1, 3 and 5 wt.% of fillers, n-Al_2O_3, w-Al_2O_3 and Fe-Al_2O_3 were added in toluene. Uniform dispersion of particles was achieved after one hour in ultrasound bath. Afterwards, 20 wt.% of EVA was added into prepared solution and mixed on 60°C on the magnetic stirrer with a rotation speed of 500 rpm for one hour. Prepared mixtures were used for UHWMPE fiber impregnation using apparatus showed in Figure 1.[29]The nozzle was changed and its dimensions were 0.4 × 1.5 mm, adapted to the dimensions of the fibers that are impregnated. To avoid composite sticking on a drum, impregnated fibers were cured with hot air on 60°C before winding.

[insert Figure 1.]

Figure1. Schematic presentation of UHMWPE impregnation process.

Characterization

The distribution of the filler particles was determined using an optical microscope and the laser particle size analyzer (PSA) Mastersizer 2000.

Morphology and shape of the particles were observed using a Mira3 Tescan field emission scanning electron microscope (FE-SEM), operated at 20 kV. The samples were previously coated with a thin gold film. The particle size and the dispersion of synthesized fillers were obtained by image analysis using the Image ProPlus 6.0 software. Images from FE-SEM were further used for measuring diameters, particle size

distribution and particle shape characterization. The laser particle size analyzer (PSA) Mastersizer 2000 was used to measure the particle size distribution, which covers the particle size range of 0.02–2000 μm.

The chemical structure of the samples was analyzed using a Fourier transform infrared spectroscopy (FT-IR) at Nicolet 6700 spectrometer (Thermo Scientific) in the attenuated total reflectance (ATR) mode with a single bounce 45 °F Golden Gate ATR accessory with a diamond crystal, and an electronically cooled DTGS detector. The spectra were the co-addition of 64 scans at 4 cm^{-1} spectral resolution, and ATR corrected. The spectrometer was equipped with OMNIC software and recorded the spectra in the wavelength range from 2.5 μm to 20 μm. Infrared spectra were recorded in transmission mode between 400 and 4.000 cm^{-1}. Fourier transform, as a mathematical process was required to convert the raw data into the actual spectrum.

Thermal analyses of samples were conducted by using a differential scanning calorimetry (DSC) and thermogravimetric analysis (TGA). The DSC measurements were conducted using a TA Instrument, TA DSC Q10 calibrated with indium standards. The temperature range was from 30 °C to 180 °C at a heating rate of 10 °C/min with a dynamic nitrogen flow of 50 ml/min. The samples were heated up to 180 °C, kept at 180 °C for 5 min to erase thermal history, and cooled down to 30 °C at the same cooling rate. A second heating was done on the each sample. The thermogravimetric analysis

was performed on a TA Instruments TGA/STD Q600 under a nitrogen gas flow (100 ml/min) between 30 °C and 600°C with a heating rate of 10 °C/min.

The tensile strength of the samples was examined using a servo hydraulic, mechanical testing machine INSTRON 1332 with control electronics FASTtrack 8800. Strain rate was 5 mm/min. All samples were of the same length and three replicates of each sample were used in the testing procedure.

Results and Discussion

The displayed measurement and results were performed in order to determine which filler contributes the most to the mechanical properties of the hybrid composite EVA/UHWMPE.

The distribution of particles

Analyzing images from the FE-SEM and processing by Image ProPlus software, the distribution of Fe-Al_2O_3 particle dimension showed submicron range of diameters achieved by sol-gel technique. More than 850 objects were analyzed in every sample of particles using the automatic object recognition algorithm. The average diameter of 0.15 μm (Table 1) was determined as most of the objects had very small dimensions. A few agglomerates have been noticed (Figure2a) as the result of lower dispersion of the particles and their joining during the calcination process, but they were recognized as individual objects by the algorithm. The presence of particle aggregates was reflected by high values of maximal observed particle diameters in Table 1. The predominance of

a great number of particles with low diameters (obvious on Figure2b) led to small mean diameter of particles, as can be seen on Figure2c. The range of measured objects is even larger than presented in Figure2c where it was between 0 and 5 μm, but the very large objects were agglomerates that are dissipated on smaller particles in the processing of the composite so the most important information is the mean value of observed individual particles.

Table 1. Statistical data of particle size distribution obtained by image analysis of Fe-Al_2O_3.

Sample		Area	Max diameter, μm	Min diameter, μm	Mean diameter, μm	Roundness
Fe-Al_2O_3	Min	0.0032	0.0565	0.0565	0.0565	1.000
	Max	542.134	55.068	12.942	26.745	176.455
	Mean	0.966	0.239	0.103	0.150	1.542
	Standard deviation	201.418	23.139	0.530	1.093	8.341

[insert Figure 2.]

Figure2.(a) FE-SEM micrograph of Fe-Al_2O_3, (b) Magnified part of Fe-Al_2O_3, FE-SEM micrograph, (c) Statistical distribution of Fe-Al_2O_3, – diameter, and (d) Particle size distribution of Fe-Al_2O_3.

Particle size distribution indicated narrow distribution of Fe-Al_2O_3 in the interval between 0.3 and 1.3 μm, with a maximum peak at 0.48 μm (Figure2d). The obtained values for particle size were in accordance with the range of distribution of mean diameter (Figure2c) suggesting that the most of agglomerates dissipated on single submicron particles.

ATR-FT-IR analysis

Chemical structure and interactions were examined using FT-IR. Spectra of the n-Al_2O_3, w-Al_2O_3 and Fe-Al_2O_3 are given in Figure3.

[insert Figure 3.]

Figure3. FT-IR spectra for fillers and hybrid composite fibers: (a) EVA/UHWMPE, (b) n-Al_2O_3, w-Al_2O_3, Fe-Al_2O_3, and (c) 1n-Al_2O_3/EVA/UHMWPE,1w-Al_2O_3/EVA/UHMWPE, 1Fe-Al_2O_3/EVA/UHMWPE hybrid composite fibers.

FT-IR identifies chemical bonds in a molecule of organic and inorganic samples by producing an infrared absorption spectrum. The resulting spectrum represents the molecular absorption, and creates a molecular fingerprint of the sample.

The scope of interest was acetate (1195 cm^{-1}), carbonyl (1731 cm^{-1}) and ethylene sequence C-H (2940 cm^{-1}) absorption region of the IR spectrum for EVA (Figure3a). The UHWMPE fibers showed characteristic absorption of ethylene segments (1470 cm^{-1}, 2950/2920 cm^{-1}, and 720 cm^{-1}).

Spectra for n-Al_2O_3, w-Al_2O_3 and Fe-Al_2O_3 fillers (Figure3b) showed changes in the intensities of absorption bands at 3300 cm^{-1} that was attributed to the presence of the O–H groups. The peak intensity of O–H groups for n-Al_2O_3 and Fe-Al_2O_3 indicated that these groups were present in a greater content on the surface than w-Al_2O_3. The function of these groups was to establish a better bonding with the composite.

The FT-IR spectra for 1n-Al_2O_3/EVA/UHMWPE, 1w-Al_2O_3/EVA/UHMWPE and 1Fe-Al_2O_3/EVA/UHMWPE (Figure 3c) indicated the characteristic peaks at 1222 cm^{-1}, 1687

cm^{-1}, and $2740cm^{-1}$ that referred to presence of C–O–C, C=O and C–H groups, respectively. Also, no vibrations of the O–H groups were noted. This indicated that these groups were used for establishing of hydrogen bonds between particles and EVA/UHWMPE hybrid composite fibers.

FE-SEM analysis

In this study, EVA/UHWMPE was compounded with the same proportions (1 wt.%) of different particles. Based on the FE-SEM images the surface properties of the fillers, matrix and UHWMPE fiber, as reinforcement, were analyzed. Dimensions of the samples (Figure4) were: length (l) 30 (±0.1) mm; width (d) 1.5 (±0.05) mm; thickness (m) 0.43(±0.03) mm. The mass proportion of UHMWPE fibers, EVA and particles in the matrix were 48.09 wt.%, 51.91 wt.% and 0.52 wt.%, respectively.

In order to obtain an insight into the impregnation quality, the cross-section of the sample was made by a sharp medical blade. To examine the morphology and the type of failure, the fractured surfaces of the samples after the tensile test were sputtered with gold and observed under SEM.

[insert Figure 4.]

Figure4. Dimensions of the samples.

The FE-SEM pattern of a fractured surface of EVA/UHWMPE composite is shown in Figure5.

[insert Figure 5.]

Figure5. The FE-SEM micrograph of unmodified EVA/UHWMPE composite:(a) Cross section before tensile test, (b) Surface of composite breakage.

Cross-sectional view in Figure5a showed that the fiber distribution in matrix was uniform, as well the wetting of UHWMPE fibers, which means that these fibers were a proper choice for EVA reinforcement due to established adhesion between these components. FE-SEM micrograph in Figure5b showed thinned UHMWPE fibers that acted as a main load bearing element. Good adhesion of EVA matrix to the fibers enabled simultaneous elongation of both components as a response to the applied load, which was followed by ductile fracture of the EVA/UHMWPE composite. Fractured surfaces of EVA/UHWMPE composite with n-Al_2O_3, w-Al_2O_3 and Fe-Al_2O_3 particles are shown in Figure6.

[insert Figure 6.]

Figure6. The FE-SEM micrograph of EVA/UHWMPE composite with: (a) 1n-Al_2O_3, (b) 1w-Al_2O_3, and (c) 1Fe-Al_2O_3.

SEM image after the tensile test of EVA/UHWMPE hybrid composite fibers with Al_2O_3 nanoparticles (Figure 6a) showed a brittle fracture. The transverse fracture surface of the matrix indicated the combined effect of mechanical interlocking between fibers and matrix with 1n-Al_2O_3. Better fiber-matrix interfacial bonding and propagation resistance across the cross sections of samples resulted in higher strengths in hybrid composite

fibers. This image was in accordance with the tensile stress results due to their higher resistance compared to the unmodified composite and w-Al_2O_3/EVA/UHWMPE.

Poor interfacial adhesion between the UHMWPE fibers and matrix is shown in Figure6. The whiskers didn't sufficiently strengthen the matrix and the fibers were pulled out. Agglomeration and segregation of whiskers were also detected. According to a separate pulled out fiber, it could be concluded that the connection between fiber and matrix was weak. The separation at the fiber-matrix interface indicated that the longitudinal cracks were nucleated at this interface.

The FE-SEM micrograph of fractured surfaces of Fe-Al_2O_3/EVA/UHWMPE showed longitudinal cracking of EVA with improved interfacial adhesion and mechanical properties of the hybrid composite fibers that caused cohesive failure of the matrix (Figure6c). It could be seen that the EVA covered the surface of UHWMPE fibers that led to higher interactions between the surfaces of the composite components.

DSC analysis

The difference in melting temperature is one of the essential indicators for the required demands of studied composites. DSC as a calorimetry method measures heat flow as a function of temperature. Heat flow can indicate structural changes driven by thermal processes. At the same time it is a good indicator of thermal active transitions such as melting temperature and glass transition temperature. Differential scanning calorimeter (DSC) thermograms of samples are shown in Figure7. From the represented

thermogram it was noticed only one melting peak for neat EVA and UHMWPE fibers at 78.4 °C and 137.2 °C, respectively.

For UHMWPE fibers, a slight difference in melting temperature (T_m) between obtained and the one reported by the producer (144-152 °C) was shown due to the environmental and storage conditions like humidity, increased storage temperature, DSC set parameters, etc[30]. EVA copolymer is a partially crystalline polymer that consists of crystalline ethylene segments and also a non-crystalline (amorphous) vinyl acetate segments.[7] An endothermic peak was typical for crystal melting of ethylene sequences in EVA copolymer[31], which was low (ΔH_{m1} = 8.708 J/g), Table 2. Unlike EVA and UHMWPE fibers, composites exhibited two clearly separated endothermic peaks corresponding to the melting phase transition of EVA and UHMWPE components. The endothermic effects were quantified by determining the total enthalpy change from the peak area for the different samples (Table 2). A significant change for neat EVA was observed at around 78 °C. According to A. Badie et al.[32], it can be associated with internal structural changes or crystallization transitions of the matrix.

The addition of fillers reduced melting enthalpy of UHMWPE fibers. Comparing to melting temperature of neat EVA, fillers slightly increased the melting temperature of the matrix (2.2%). When the melting point of EVA/UHMWPE and hybrid composites were compared, it can be concluded that no change in melting point was observed by inducing particles. The main change in EVA phase melting transition was noticed by

melting enthalpy. Sharp decrease in melting enthalpy (ΔH_{m1}) for 52.9-65.5% suggested large-scale structural changes due to disturbance of polyethylene segment packing by the introduction of reinforcement as UHMWPE and particles. Maintained value for T_{m1} enabled preserved mechanical properties of EVA matrix concerning the elongation of the composites and the amount of absorbed load.

However, a change of the melting temperature of UHMWPE phase didn't follow specific order and the values for hybrid composite were similar. Melting enthalpy of UHMWPE phase for hybrid composites showed significant differences. The highest melting enthalpy of UHMWPE phase (ΔH_{m2}) for hybrid composite 1Fe-Al_2O_3/EVA/UHMWPE showed the structural arrangement of reinforcement. Negligible UHMWPE melting point decrement (2.2%) in composites may be prescribed to structural changes due to disturbance of surface polyethylene sequences by the processing of hybrid composites and thus the use value of composites wasn't affected by the use of presented technology.

[insert Figure 7.]

Figure7. DSC thermograms of EVA, UHMWPE fibers and composite fibers.

Table 2. Temperatures and enthalpies obtained from DSC thermograms.

Samples	T_{m1} (°C) (EVA phase)	ΔH_{m1} (J/g) (EVA phase)	T_{m2} (°C) (UHMWPE phase)	ΔH_{m2} (J/g) (UHMWPE phase)
UHMWPE			137.2	78.2
EVA	78.4	8.7		
EVA/UHMWPE	79.7	3.6	133.8	24.7
1n-Al_2O_3/EVA/UHMWPE	80.0	4.1	134.2	20.9
1w-Al_2O_3/EVA/UHMWPE	79.5	3.0	134.2	24.4
1Fe-Al_2O_3/EVA/UHMWPE	80.1	3.3	134.2	32.3

Overall endothermic enthalpy for six samples was classified in the following rank: UHMWPE (78.2 J/g)>1Fe-Al_2O_3/EVA/UHMWPE (35.6 J/g)>EVA/UHMWPE (28.3 J/g) >1w-Al_2O_3/EVA/UHMWPE (27.4 J/g) >1n-Al_2O_3/EVA/UHMWPE(24.9 J/g)> EVA (8.7 J/g).

Thermal degradation study of hybrid composite fibers

Thermogravimetric curves of EVA, UHMWPE fibers and composites are presented on Figure8a. Thermal stability was evaluated at decomposition temperatures at 5% of weight loss ($T_{0.05}$) and at 50% of weight loss ($T_{0.5}$).

Degradation of EVA, as the matrix, was followed by two degradation steps. The first step was a deacetylation process that started at 286.5 °C and completed at 381.5 °C. In this temperature range, chain fragments as carbon monoxide, carbon dioxide ketene and water were probably formed during the thermal decomposition of the acetic acid.[33] Within this interval EVA yielded ethylene and acetic acid.[34]

At the first point ($T_{0.05}$), the highest temperature of degradation occurred for UHMWPE fibers and 1Fe-Al_2O_3/EVA/UHMWPE, 408.1 °C and 383.3 °C, respectively. In interval from 156.6 °C to 351.4 °C, 1Fe-Al_2O_3/EVA/UHMWPE showed higher stability than other samples.

On the second point ($T_{0.5}$), all of the samples displayed similar degradation profiles. The second step referred to degradation of the EVA backbone (chain scission within the interval of 400-500 °C).[35,36] It was noticeable that the presence of fillers in EVA improved the thermal stability of the matrix. According to the results presented in Table 3, decomposition temperatures $T_{0.05}$ and $T_{0.5}$ showed that the reinforcement of EVA matrix improved the thermal stability.[30] The experimental results (Figure8a) showed that the addition of fillers improved thermal stability and prolonged degradation temperatures.

The higher mass residual for neat EVA (3.27%) was associated with networking of EVA polymer due to instability and formation of double bonds after the degradation. M. C. Costache et al. suggested that in the first step of degradation, acetic acid loss was related to the presence of hydroxyl groups on the edges of fillers.[37] That was in accordance with the results obtained for neat EVA. Results for hybrid composite fibers proved that the lowest mass weight loss was for 1n-Al_2O_3/EVA/UHMWPE and 1Fe-Al_2O_3/EVA/UHMWPE. Degradation processes of EVA matrix, UHMWPE fibers and UHMWPE/EVA hybrid composite fibers were represented by DTG curves in

Figure8(b). For all samples except UHMWPE fibers, degradation occurred at approximately 351 °C. The final point was similar for all samples and it is shown in Table 3.

Table 3. Temperatures obtained from TG/DTG diagrams.

Samples	TG			DTG	
	$T_{0.05}$ (°C)	$T_{0.5}$ (°C)	Mass res. (%)	T_1 (°C)	T_2 (°C)
UHMWPE	408.1	477.5	0.421		480.9
EVA	347.6	471.1	3.277	364.1	481.6
EVA/UHMWPE	345.7	471.7	3.243	352.3	477.2
1n-Al_2O_3/EVA/UHMWPE	357.1	471.8	0.009	352.9	478.4
1w-Al_2O_3/EVA/UHMWPE	349.5	472.7	1.154	351.6	480.8
1Fe-Al_2O_3/EVA/UHMWPE	383.3	472.4	0.110	351.6	478.5

[insert Figure 8.]

Figure8.TG (a) and DTG (b) diagrams for EVA, UHMWPE fibers and hybrid composite fibers.

Tensile test

Tests were performed in order to determine tensile strength and modulus of elasticity of EVA/UHMWPE hybrid composite fibers with different fillers and their mass fractions. The values of tensile strength of different concentration of fillers are presented in Figure9. The highest values for different filers and concentrations were for 1Fe-Al_2O_3/EVA/UHMWPE (823.02 MPa).

[insert Figure 9.]

Figure9. Tensile test results of hybrid composites.

According to the results given in Figure9, dependence of tensile stress on relative displacement of four samples of 1n-Al_2O_3/EVA/UHMWPE, 1w-Al_2O_3/EVA/UHMWPE, 1Fe-Al_2O_3/EVA/UHMWPE and EVA were presented on Figure10. The addition of 1 wt.% of any of the used fillers showed that the highest tensile stress was for 1Fe-Al_2O_3/EVA/UHMWPE.

[insert Figure 10.]

Figure 10. Tensile test diagram for hybrid composite fibers with 1 wt.% of fillers.

The measured values of tensile strength for 1n-Al_2O_3/EVA/UHMWPE, 1w-Al_2O_3/EVA/UHMWPE and 1Fe-Al_2O_3/EVA/UHMWPE compared to EVA/UHMWPE showed an increase of 63.0, 31.9 and 100.7%, respectively. The significant improvement in the mechanical properties could be attributed to the strong interaction between the hydroxyl groups of Fe-Al_2O_3 and EVA because of the sintering process at lower temperatures, where OH groups partially remained on alumina surface, so the better binding with EVA was expected. Formation of agglomerates of w-Al_2O_3 resulted in a reduction of tensile strength value.

Resulting values of the modulus of elasticity (Figure11) had a different trend. The highest value of modulus of elasticity shown for 1n-Al_2O_3/EVA/UHMWPE indicated the increase of rigidity of the hybrid composites, resulting brittle failure of the matrix seen in the SEM image (Figure5a). A larger area under the stress-displacement curve for the 1Fe-Al_2O_3/EVA/UHMWPE sample was a consequence of more resilient composite

obtained that can absorb a higher amount of tensile energy. Such a behavior was reflected by lower modulus of elasticity. Alumina fillers in a form of whiskers in a sample 1w-Al_2O_3/EVA/UHMWPE caused the lowest mechanical properties in relation to other hybrid composites, while the modulus of elasticity was lower than the one obtained for EVA without particle reinforcement (EVA/UHMWPE). This behavior may be explained with higher amount of aggregates in the matrix that disabled interaction with the main reinforcement of the composites – UHMWPE.

[insert Figure 11.]

Figure11. Effect of the composition of the samples on the modulus of elasticity.

Conclusions

In this article, experimental results were presented for UHWMPE fibers as reinforcement with 1, 3 and 5 wt.% of alumina nanoparticles, whiskers and iron doped alumina particles as fillers in EVA matrix. The tensile results obtained for hybrid composites with 1 wt.% of particles indicated that the optimal weight percentage was used which was compliant with the literature.

In comparison with other used commercial fillers, Fe-Al_2O_3 showed a submicron particle size distribution. Average diameter of 0.15 μm had a significant effect on the mechanical properties due to better dispersion and distribution in the matrix.

FE-SEM analysis proved the best fiber-matrix interfacial adhesion for 1-Fe-Al_2O_3/EVA/UHMWPE due to resilient longitudinal cracking of EVA that confirmed excellent bonding.

This was in agreement with tensile test results where1-Fe-Al_2O_3/EVA/UHMWPE showed improved mechanical properties in comparison with hybrid composite fibers with nanoparticles or whiskers.

FT-IR spectra indicated better interactions between Fe-Al_2O_3 and matrix due to established hydrogen bonds.

Presented results from the FT-IR, FE-SEM, and tensile stress analysis showed that in comparison with commercial available aluminum oxide nanoparticles with particle size less than 50 nm and alumina whiskers (diameter 2 – 4 nm × 400 nm), synthesized iron oxide doped alumina particles were the best choice for hybrid reinforcement of EVA/UHMWPE composites.

DSC analysis presented the highest melting enthalpy of UHMWPE phase (32.3 J/g) for 1Fe-Al_2O_3/EVA/UHMWPE, which indicated that the composite with the best structural arrangement of main reinforcement was obtained.

TG/DTG curves represented that degradation process temperatures of EVA matrix, UHMWPE fibers and UHMWPE/EVA composites were similar for all samples except UHMWPE fibers. Temperature of onset of degradation ($T_{0.05}$) showed that the particles improved thermal stability of EVA/UHMWPE composites, where the highest value was

observed for UHMWPE fibers. It was interesting to notice that iron doped particles improved thermal stability of hybrid composite until 350 °C even compared to UHMWPE fibers.

The incorporation of different combination of fillers had, in general, a significant improvement effect on modulus of elasticity causing different type of composite failure. The highest modulus of elasticity for composite with alumina nanoparticles (1n-Al_2O_3/EVA/UHMWPE) was followed by brittle matrix failure. The most resilient hybrid composite with iron doped alumina represented the composite that was able to absorb the highest amount of tensile energy.

It can be concluded that EVA/UHWMPE hybrid composite fibers with Fe-Al_2O_3 particles were superior to those of EVA/UHMWPE, or hybrid composites with Al_2O_3 nanoparticles or whiskers.

Acknowledgment

The authors wish to acknowledge the financial support from the Ministry of Education, Science and Technological Development of the Republic of Serbia through Project No. TR 34011.

References

1. Lin SP, Han JL, Yeh JT, Chang FC, Hsieh KH. Surface Modification and Physical Properties of Various UHMWPE-Fiber-Reinforced Modified Epoxy Composites. *J Appl*

*Polym Sci*2007;104:655–665. DOI: 10.1002/app.25735

2. Razavi-Nouri M, Karami M. Effect of rubber content on morphology and thermal and rheological behaviors of acrylonitrile-butadiene rubber/poly(ethylene-co-vinyl acetate)/organoclay nanocomposites. *Polym (United Kingdom)*2014;55(26):6940–7. DOI: 10.1016/j.polymer.2014.10.050

3. Cavodeau F, Sonnier R, Otazaghine B, Lopez-Cuesta JM, Delaite C. Ethylene-vinyl acetate copolymer/aluminium trihydroxide composites: A new method to predict the barrier effect during cone calorimeter tests. *Polym Degrad Stab*2015;120:23–31. DOI: 10.1016/j.polymdegradstab.2015.05.021

4. El Hage R, Viretto A, Sonnier R, Ferry L, Lopez-Cuesta JM. Flame retardancy of ethylene vinyl acetate (EVA) using new aluminum-based fillers. *Polym Degrad Stab*2014;108:56–67. DOI: 10.1016/j.polymdegradstab.2014.05.029

5. Chalykh AE, Stepanenko VY, Shcherbina AA, Balashova EG. Adhesive properties of ethylene and vinyl acetate copolymers. *Polym Sci Ser D*2009;2(1):8–15. DOI: 10.1134/S199542120901002X

6. Sviridenok AI, Zharin AL, Krautsevich AU, Tyavlovsky AK. The effect of high-dispersion fillers on adhesive and frictional properties of ethylene-vinyl acetate copolymer. *J Frict Wear*2014;35(4):255–62.DOI: 10.3103/S1068366614040114

7. Shi XM, Zhang J, Jin J, Chen SJ. Non-isothermal crystallization and melting of ethylene-vinyl acetate copolymers with different vinyl acetate contents. *Express Polym Lett*2008;2(9):623–9. DOI: 10.3144/expresspolymlett.2008.75

8. Soto Puente JA, Fatyeyeva K, Marais S, Dargent E. Multifunctional hydrolyzed EVA membranes with tunable microstructure and water barrier properties. *J Memb Sci* 2015;480:93–103. DOI: 10.1016/j.memsci.2015.01.008

9. Zhang Y, Gu J, Tan H, Shi J, Di M, Zuo Y, et al. Preparation and characterization of film of poly vinyl acetate ethylene copolymer emulsion. *Appl Surf Sci*2013;276:223–8. DOI: 10.1016/j.apsusc.2013.03.071

10. Kango S, Kalia S, Celli A, Njuguna J, Habibi Y, Kumar R. Surface modification of inorganic nanoparticles for development of organic-inorganic nanocomposites - A review. *Prog Polym Sci*2013;38(8):1232–61. DOI: 10.1016/j.progpolymsci.2013.02.003

11. Marissen R. Design with Ultra Strong Polyethylene Fibers. *Mater Sci Appl*2011;2(May):319–30. DOI: 10.4236/msa.2011.25042

12. Chang BP, Md. Akil H, Bt. Md. Nasir R. Comparative study of micro- and nano-ZnO reinforced UHMWPE composites under dry sliding wear. Wear2013;297(1–2):1120–7. DOI: 10.1016/j.wear.2012.11.083

13. Hsieh AJ, Chantawansri TL, Hu W, Cain J, Yu JH. New insight into the influence of molecular dynamics of matrix elastomers on ballistic impact deformation in UHMWPE composites. *Polym (United Kingdom)* 2016;95:52–61. DOI: 10.1016/j.polymer.2016.04.048

14. McDaniel PB, Deitzel JM, Gillespie JW. Structural hierarchy and surface morphology of highly drawn ultra high molecular weight polyethylene fibers studied by atomic force microscopy and wide angle X-ray diffraction. *Polymer*2015;69:148–58. DOI: 10.1016/j.polymer.2015.05.010

15. Kang Y-A, Oh S-H, Park JS. Properties of UHMWPE fabric reinforced epoxy composite prepared by vacuum-assisted resin transfer molding. *Fibers Polym* 2015;16(6):1343–8. DOI: 10.1007/s12221-015-1343-8

16. Chand N, Dwivedi UK, Sharma MK. Development and tribological behaviour of UHMWPE filled epoxy gradient composites. *Wear* 2007;262(1–2):184–90. DOI:10.1016/j.wear.2006.04.012

17. Oliveira M, Machado AV. Preparation and characterization of ethylene-vinyl acetate nanocomposites: Enhanced flame retardant. *Polym Int* 2013;62(12):1678–83.DOI: 10.1002/pi.4466

18. Jin B, Zhang W, Sun G, Gu H-B. Fabrication and characterization of ethylene-vinyl acetate copolymer/Al_2O_3nanocomposites. *J Ceram Process Res* 2007;8(5):336–40.

19. Baskaran R, Sarojadevi M, Vijayakumar CT. Unsaturated polyester nanocomposites filled with nano alumina. *J Mater Sci*2011;46(14):4864–71.DOI: 10.1007/s10853-011-5398-7

20. Chee CY, Song NL, Abdullah LC, Choong TSY, Ibrahim A, Chantara TR. Characterization of mechanical properties: Low-density polyethylene nanocomposite using nanoalumina particle as filler. *J Nanomater*2012;2012.

DOI:10.1155/2012/215978

21. Mallakpour S, Khadem E. Recent development in the synthesis of polymer nanocomposites based on nano-alumina. *Prog Polym Sci* 2014;51:74–93. DOI: 10.1016/j.progpolymsci.2015.07.004

22. Milanović P, Dimitrijević M, Jančić Heinemann R, Rogan J, Stojanović DB, Kojović A, et al. Preparation of low cost alumina nanofibers via electrospinning of aluminium chloride hydroxide/poly (vinyl alcohol) solution. *Ceram Int* 2013;39(2):2131–4. DOI: 10.1016/j.ceramint.2012.07.062

23. Opelt CV, Becker D, Lepienski CM, Coelho LAF. Reinforcement and toughening mechanisms in polymer nanocomposites –Carbon nanotubes and aluminium oxide.*Composites Part B*2015;75:119–26. Available from: http://dx.doi.org/10.1016/j.compositesb.2015.01.019

24. Wetzel B, Rosso P, Haupert F, Friedrich K. Epoxy nanocomposites - fracture and toughening mechanisms. *Eng Fract Mech* 2006;73(16):2375–98. DOI: 10.1016/j.engfracmech.2006.05.018

25. Cho J, Joshi MS, Sun CT. Effect of inclusion size on mechanical properties of polymeric composites with micro and nano particles. *Compos Sci Technol* 2006;66(13):1941–52. DOI: 10.1016/j.compscitech.2005.12.028

26. Opelt CV, Coelho LAF. Reinforcement and toughening mechanisms in polymer nanocomposites - Reinforcement effectiveness and nanoclay nanocomposites. *Mater Chem Phys* 2015;169:179–85.DOI: 10.1016/j.matchemphys.2015.11.047

27. Heydari-Meybodi M, Saber-Samandari S, Sadighi M. A new approach for prediction of elastic modulus of polymer/nanoclay composites by considering interfacial debonding: Experimental and numerical investigations. *Compos Sci Technol* 2015;117:379–85. DOI: 10.1016/j.compscitech.2015.07.014

28. Alzarrug FA, Dimitrijević MM, Jančić Heinemann RM, Radojević V, Stojanović DB, Uskoković PS, et al. The use of different alumina fillers for improvement of the mechanical properties of hybrid PMMA composites. *Mater Des* 2015;86:575–81. DOI: 10.1016/j.matdes.2015.07.069

29. Tomić NZ, Međo BI, Stojanović DB, Radojević VJ, Rakin MP, Jančić-Heinemann RM, et al. A rapid test to measure adhesion between optical fibers and

ethylene–vinyl acetate copolymer (EVA). *Int J Adhes Adhes*2016;68:341–50. DOI: 10.1016/j.ijadhadh.2016.04.012

30. An M, Xu H, Lv Y, Duan T, Tian F, Hong L, et al. Ultra-strong gel-spun ultra-high molecular weight polyethylene fibers filled with chitin nanocrystals. *RSC Adv* 2016;6(25):20629–36. DOI: 10.1039/C5RA25786G

31. Stark W, Jaunich M. Investigation of Ethylene/Vinyl Acetate Copolymer (EVA) by thermal analysis DSC and DMA. *Polym Test* 2011;30(2):236–42. DOI: 10.1016/j.polymertesting.2010.12.003

32. Badiee A, Ashcroft IA, Wildman RD. The thermo-mechanical degradation of ethylene vinyl acetate used as a solar panel adhesive and encapsulant. *Int J Adhes Adhes*2016;68:212–8. DOI: 10.1016/j.ijadhadh.2016.03.008

33. Marín ML, Jiménez A, López J, Vilaplana J. Thermal degradation of ethylene (vinyl acetate) Kinetic analysis of thermogravimetric data. *J Therm Anal*1996;47(1):247–58. DOI: 10.1007/BF01982703

34. Osayemwenre GO, Meyer EL. Thermal Decomposition of Eva Composite Encapsulant of Single Junction Amorphous Silicon Photovoltaic (Pv) Module. *J Ovonic Res* 2014;10(6):221–9.

35. Lizymol PP, Thomas S. Thermal behaviour of polymer blends: a comparison of the thermal properties of miscible and immiscible systems. *Polym Degrad Stab* 1993;41(1):59–64. DOI: 10.1016/0141-3910(93)90061-M

36. Mochane MJ, Luyt AS. The Effect of Expanded Graphite on the Thermal Stability,Latent Heat, and Flammability Properties of EVA/Wax PhaseChange Blends. *Polymer Engineering and Science* 2015; DOI: 10.1002/pen.24063

37. Costache MC, Jiang DD, Wilkie CA. Thermal degradation of ethylene-vinyl acetate coplymer nanocomposites. *Polymer* 2005;46(18):6947–58. DOI: 10.1016/j.polymer.2005.05.084

FIGURE CAPTIONS

Figure1. Schematic presentation of UHMWPE impregnation process.
Figure2.(a) FE-SEM micrograph of Fe-Al_2O_3, (b) Magnified part of Fe-Al_2O_3, FE-SEM micrograph, (c) Statistical distribution of Fe-Al_2O_3, – diameter, and (d) Particle size distribution of Fe-Al_2O_3.
Figure3. FT-IR spectra for fillers and hybrid composite fibers: (a) EVA/UHWMPE, (b) n-Al_2O_3, w-Al_2O_3, Fe-Al_2O_3, and (c) 1n-Al_2O_3/EVA/UHMWPE,1w-Al_2O_3/EVA/UHMWPE, 1Fe-Al_2O_3/EVA/UHMWPE hybrid composite fibers.
Figure4. Dimensions of the samples.
Figure5. The FE-SEM micrograph of unmodified EVA/UHWMPE composite:(a) Cross section before tensile test, (b) Surface of composite breakage.
Figure6. The FE-SEM micrograph of EVA/UHWMPE composite with: (a) 1n-Al_2O_3, (b) 1w-Al_2O_3,and (c) 1Fe-Al_2O_3.
Figure7. DSC thermograms of EVA, UHMWPE fibers and composite fibers.
Figure8.TG (a) and DTG (b) diagrams for EVA, UHMWPE fibers and hybrid composite fibers.
Figure9. Tensile test results of hybrid composites.
Figure 10. Tensile test diagram for hybrid composite fibers with 1 wt.% of fillers.
Figure11. Effect of the composition of the samples on the modulus of elasticity.

TABLE CAPTIONS

Table 1. Statistical data of particle size distribution obtained by image analysis of Fe-Al_2O_3.
Table 2. Temperatures and enthalpies obtained from DSC thermograms.
Table 3. Temperatures obtained from TG/DTG diagrams.

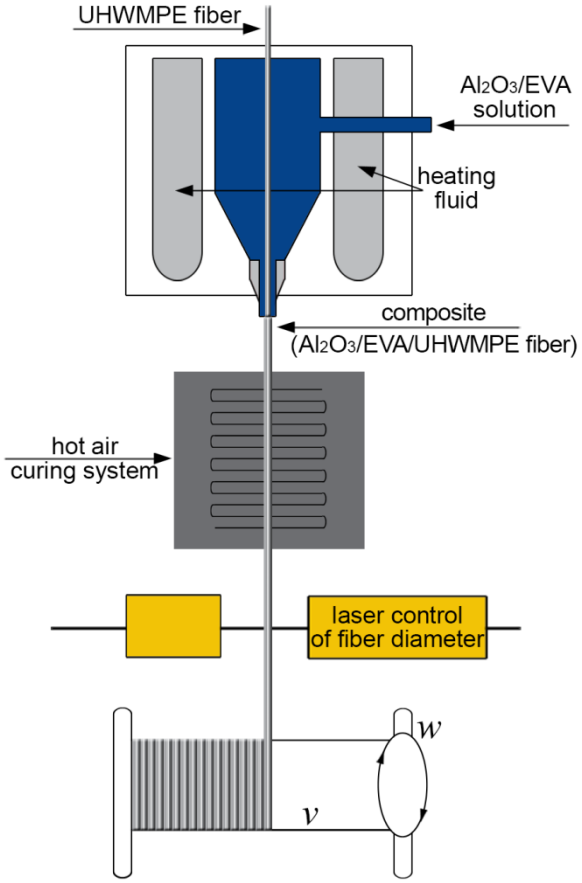
UHWMPE fiber
Al2O3/EVA
solution
heating
fluid
composite
(Al2O3/EVA/UHWMPE fiber)
hot air
curing system
laser control
of fiber diameter
w
v

Figure 1

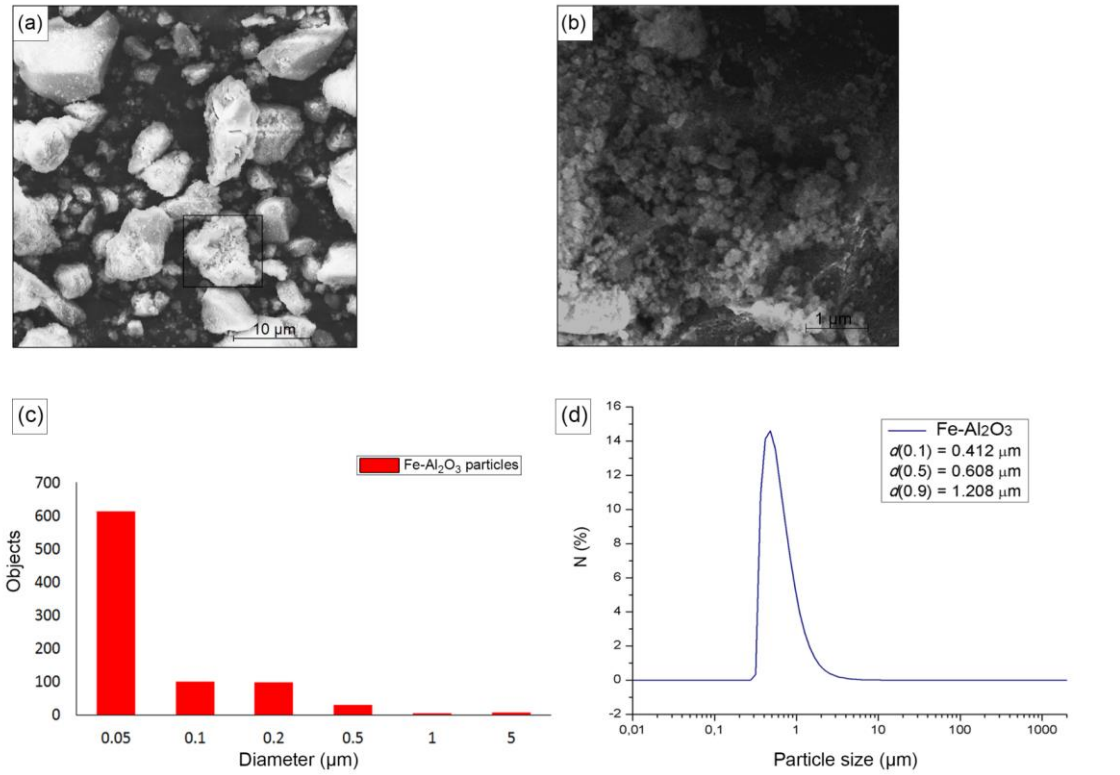

Figure 2

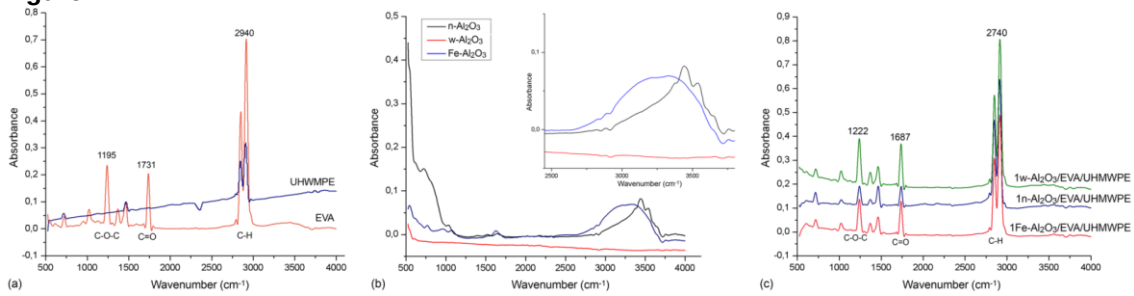

Figure 3

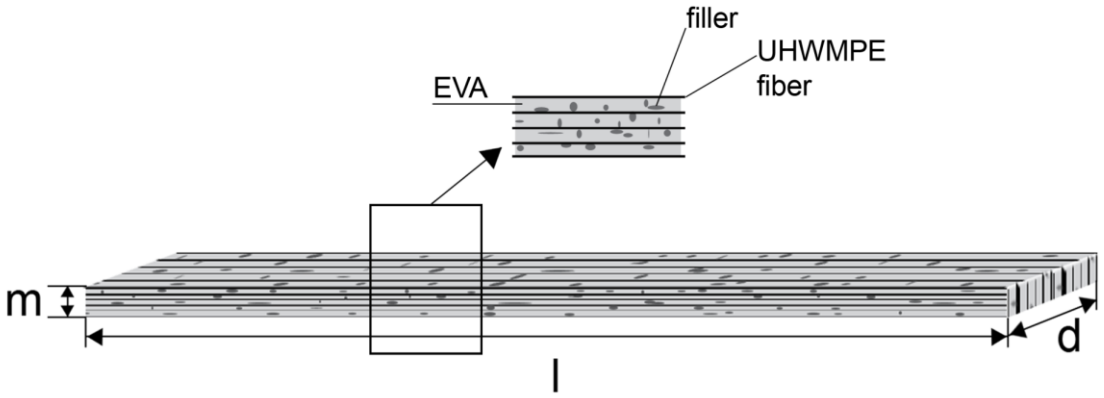

Figure 4

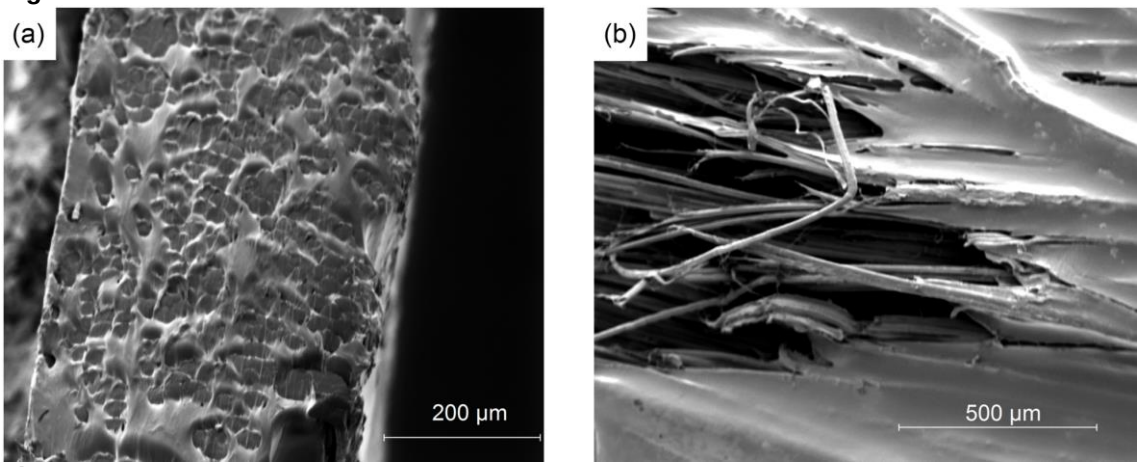

Figure 5

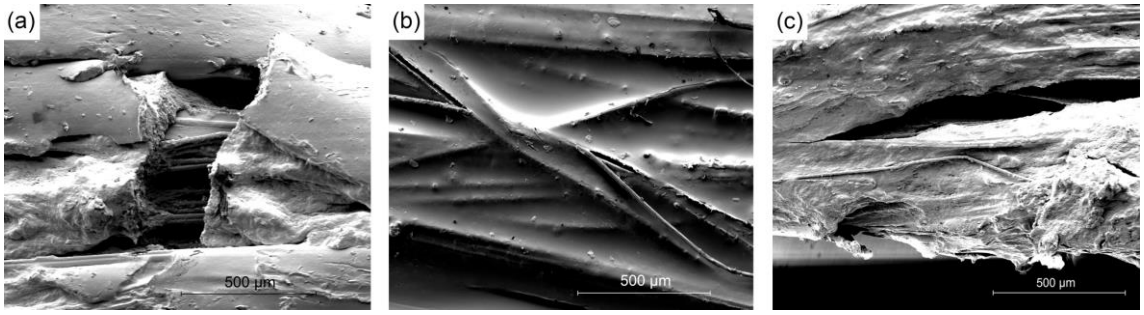

FIgure 6

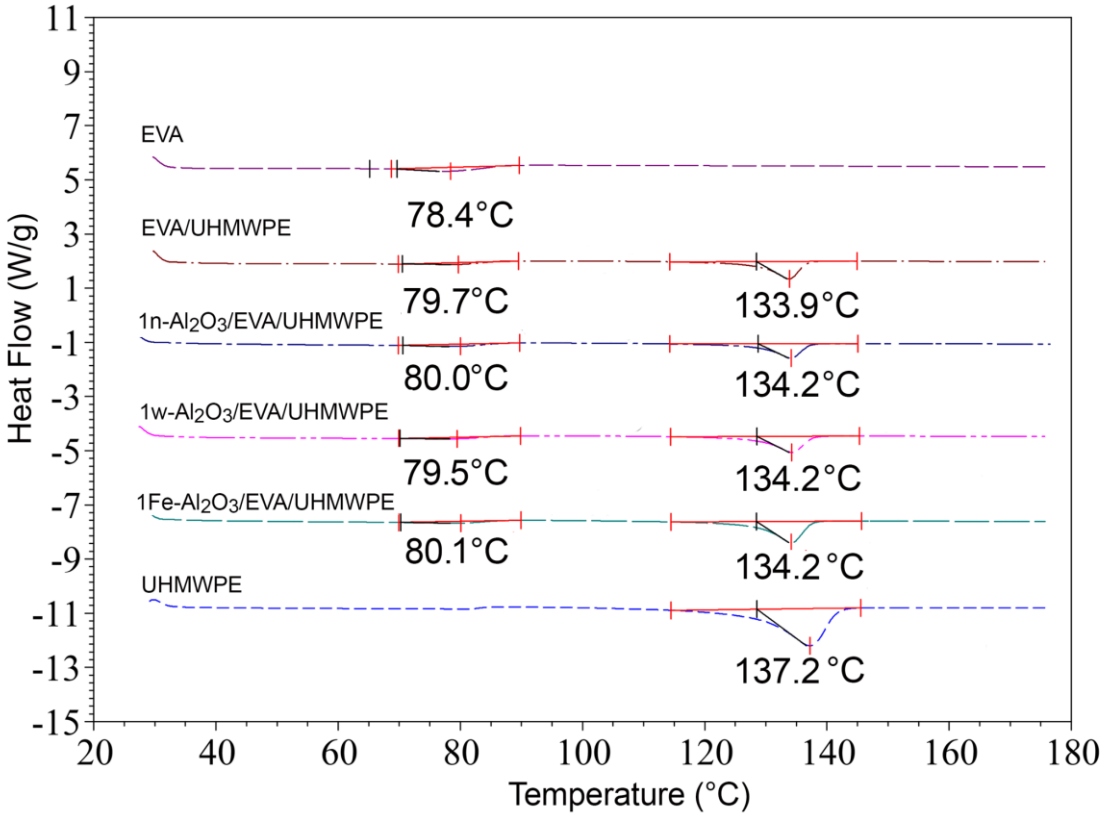

Figure 7

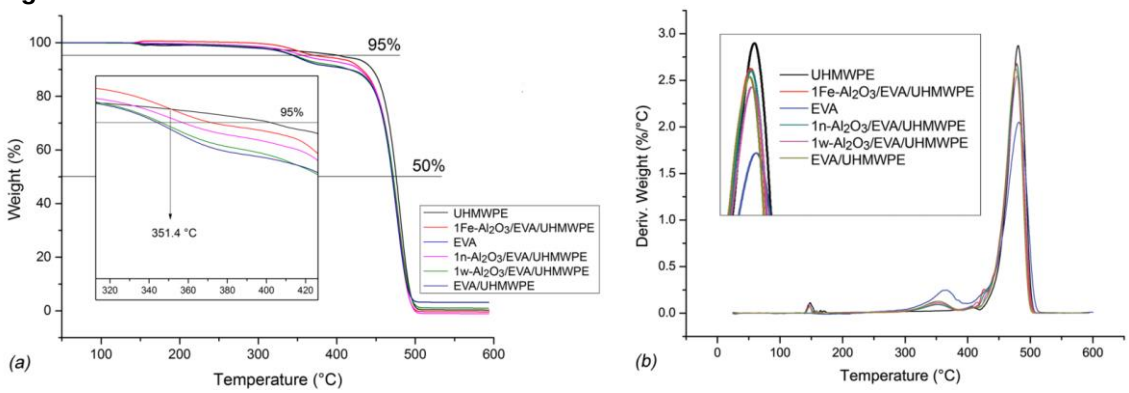

Figure 8

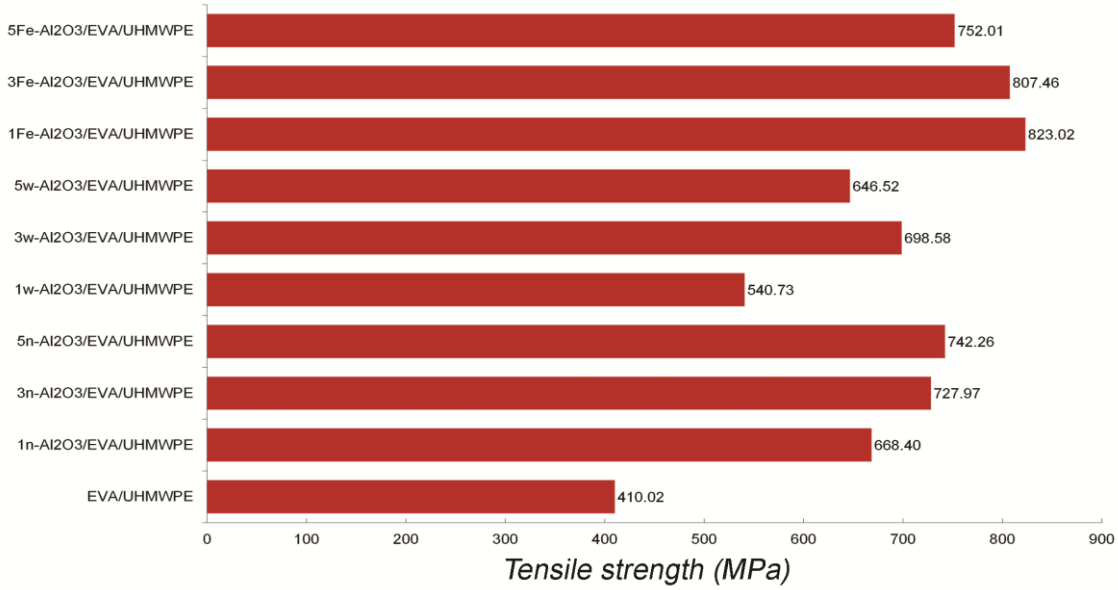
5Fe-Al2O3/EVA/UHMWPE
752.01
3Fe-Al2O3/EVA/UHMWPE
807.46
1Fe-Al2O3/EVA/UHMWPE
823.02
5w-Al2O3/EVA/UHMWPE
646.52
3w-Al2O3/EVA/UHMWPE
698.58
1w-Al2O3/EVA/UHMWPE
540.73
5n-Al2O3/EVA/UHMWPE
742.26
3n-Al2O3/EVA/UHMWPE
727.97
1n-Al2O3/EVA/UHMWPE
668.40
EVA/UHMWPE
410.02
0
100
200
300
400
500
600
700
800
900
Tensile strength (MPa)

Figure 9

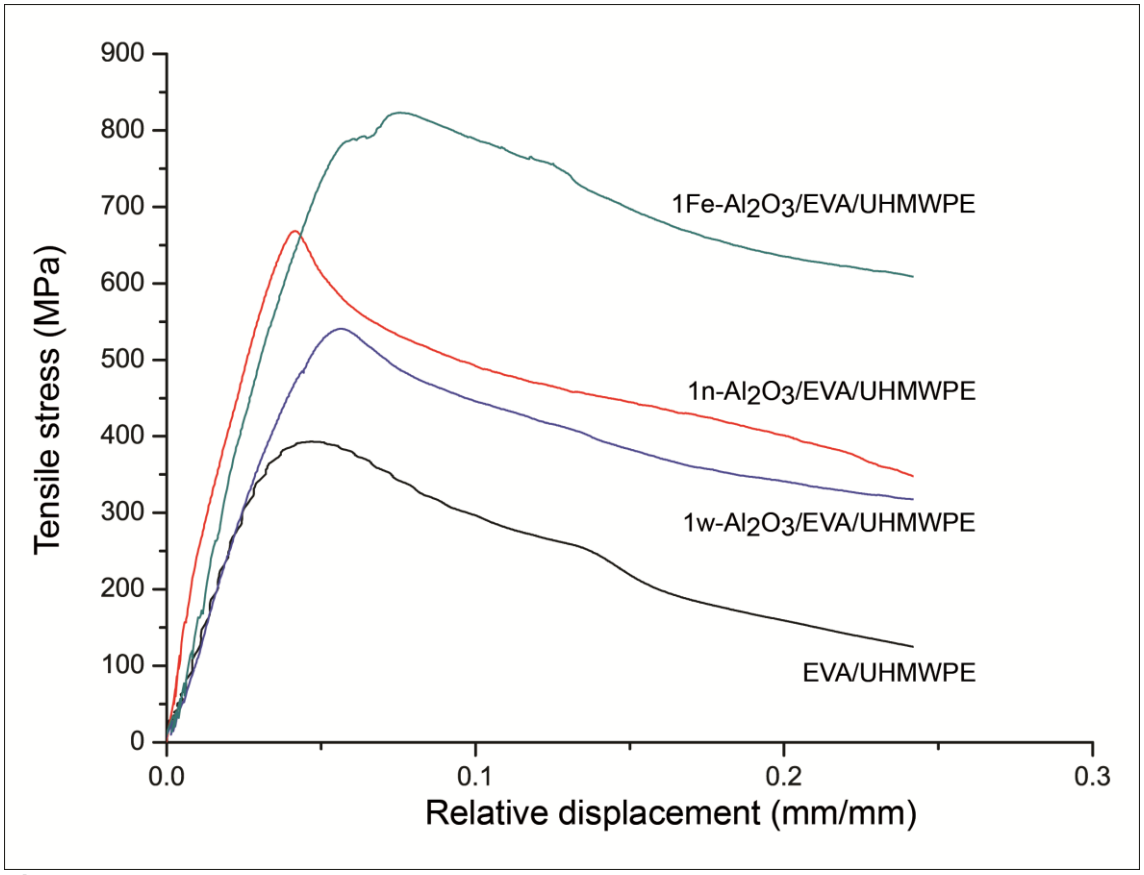
900
800
700
600
500
400
300
200
100
0
Tensile stress (MPa)
0.0
0.1
0.2
0.3
Relative displacement (mm/mm)
1Fe-Al2O3/EVA/UHMWPE
1n-Al2O3/EVA/UHMWPE
1w-Al2O3/EVA/UHMWPE
EVA/UHMWPE

Figure 10

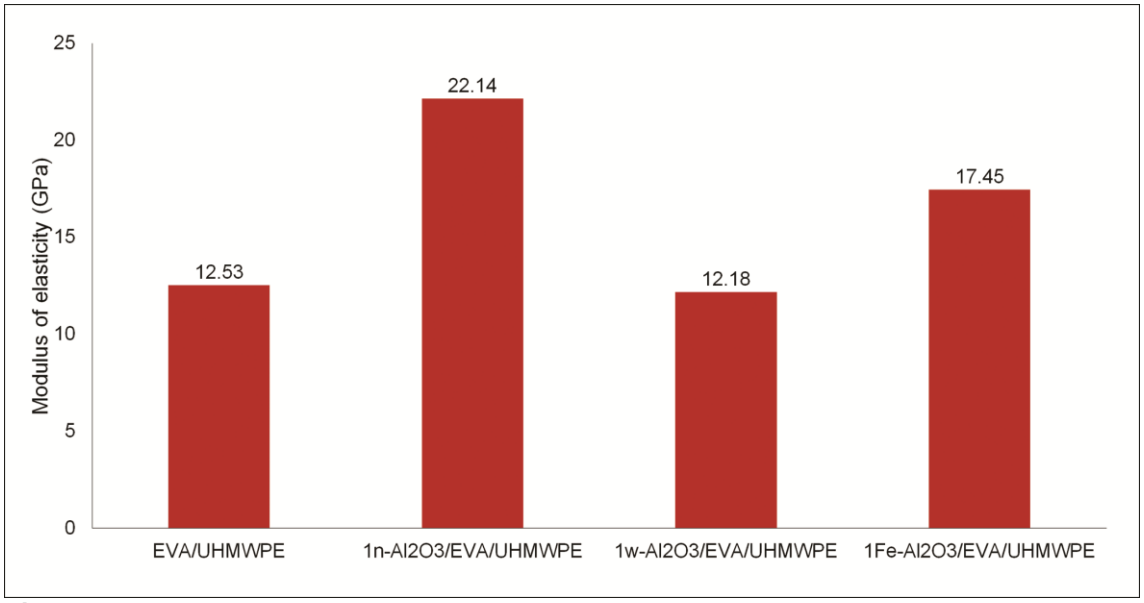
25
20
15
10
5
0
Modulus of elasticity (GPa)
12.53
22.14
12.18
17.45
EVA/UHMWPE
1n-Al2O3/EVA/UHMWPE
1w-Al2O3/EVA/UHMWPE
1Fe-Al2O3/EVA/UHMWPE

Figure 11